Dynamic percolation in fluorinated water-in-oil microemulsions

Cecilia M.C. Gambi, M. Grazia Giri, Marcello Carlà, and Donatella Senatra
Department of Physics, University of Florence and INFM, Largo E. Fermi 2, 50125 Florence, Italy

Alba Chittofrati
Ausimont, R&D Centre, Colloid Laboratory, Via San Pietro 50, 20021 Bollate, Milan, Italy
(Received 10 February 1997)

Dielectric spectroscopy was performed to study fluorinated water-in-oil microemulsions with perfluoropolyether surfactant and oil. The phase diagram experimental path, with a water to surfactant molar ratio equal to 11, was chosen as the most suitable for detecting a percolation phenomenon that occurs in the system. The study of the percolation phenomenon as a function of temperature was presented in Phys. Rev. E **50**, 1313 (1994). In this work, the concentration dependence of both the static dielectric constant and Ohmic conductivity, as well as the frequency dependence of the complex dielectric constant, are reported. The results show that the percolation is dynamic throughout both the composition and the temperature range in which the samples are monophasic. [S1063-651X(97)12809-4]

PACS number(s): 64.70.Ja, 77.22.−d, 82.70.Dd, 61.25.Hq

I. INTRODUCTION

It was recently reported that fluorinated water-in-oil microemulsions composed of perfluoropolyether compounds (PFPE) show a percolation phenomenon [1]. These microemulsions were studied by phase diagram, conductivity measurements, light scattering, nuclear magnetic resonance, dielectric investigation, etc. (see Ref. [1] for a complete list of references). The ternary system water W, fluorinated surfactant S, and fluorinated oil O, shows a large monophasic domain of homogeneous, transparent, isotropic samples [2]. A light scattering investigation [3] gave reliable results for the dilute microemulsions, $\phi<0.10$, where ϕ is the volume fraction of the dispersed phase (water plus surfactant, over total), assuming the dispersed phase composed of water droplets coated by surfactant molecules. Droplets on nanometer scale were identified at water to surfactant molar ratio (W/S) higher than 6 [3]. It was experimentally established that, at constant W/S ratio, increasing the oil content (diluting by oil) [4], the droplets maintain a constant radius. Spherical shapes were hypothesized, as no experimental evidence of depolarized light was found, and the polydispersity was very low (10%). Hydrodynamic radius from 3 to 6 nm, and dynamic second virial coefficients from -20 to 0 were found [3], indicating that the droplets interact via a potential composed of a strong repulsive part (steric repulsion) and an attractive part. The main goal of the dielectric study [1] was to characterize the microemulsion structure in the concentrated region (high ϕ values) where other techniques cannot help. Results of the dielectric investigation (measurements of Ohmic conductivity and static dielectric constant), performed as a function of temperature on samples with different concentrations (at constant W/S=11), elucidated that fluorinated microemulsions show a percolation phenomenon, mainly of dynamic nature. In agreement with the theory [5,6] and with many similar results on hydrogenated microemulsions [7–19], the interpretation of the dielectric results of Ref. [1] supports the following description of the microemulsion system. In the dilute region, the conduction mechanism may be interpreted in terms of droplet charge fluctuations [20]. Although the droplets are, on average, electrically neutral, they can carry excess charge due to spontaneous thermal composition fluctuations. The migration of these charged droplets in an electric field is the main conductivity mechanism in dilute water-in-oil microemulsion systems. On approaching the percolation thermal threshold from below (i.e., increasing the temperature), for all the samples studied, critical exponents typical of dynamic percolation were found [1]. This implies that the increase of thermal energy induces the formation of transient clusters because of attractive interactions between droplets. Surfactant ions and counterions can migrate from droplet to droplet within a cluster. The exchange process between two droplets consists of a diffusional approach of two droplets, followed by the exchange of ionic species (via surfactant molecules jumping from one droplet to another), and by diffusional separation of the droplets. When the temperature increases and clusters of droplets are formed, on approaching the thermal threshold, a steep increase in the carrier diffusion is expected, because of a transition from a regime of transport dominated by droplet motion and cluster rearrangement to one dominated by the motion of charge carriers on a large connected cluster of droplets. The latter depends as a power law on the rate of cluster rearrangement, i.e., on the time for a large cluster to be broken up into two smaller ones, or for two clusters to fuse into a single larger one. At threshold, at least one cluster of droplets connects the system from one electrode to the other. A recent detailed analysis and estimation of the relaxation times of the processes involved at microscopic level in the dynamic percolation process for a sodium bis(2-ethylhexyl) sulfosuccinate (AOT) based water-in-oil microemulsion, was reported in Ref. [21]. We have to point out that below the thermal threshold, for the fluorinated microemulsions, the process was found to be of dynamic type in the explored ϕ interval from 0.205 to 0.501 at W/S=11. Thus the previous description of the phenomenon applies for either the diluted and concentrated microemulsions, indicating that the system is composed of interacting

droplets which forms clusters without droplets coalescence [1]. However, above the thermal threshold, the droplets form a growing number of clusters (dynamic percolation), or coalesce (bicontinuous microemulsion). Above threshold, the percolation was found to be dynamic at $\phi=0.361$, 0.395, and 0.462, and static at $\phi=0.205$, 0.327, and 0.501 [1].

In this paper we report the concentration dependence of both the static dielectric constant and Ohmic conductivity of microemulsion samples with W/S=11, as well as the frequency dependence of the microemulsions complex permittivity at different concentrations and temperatures. In principle, a microemulsion sample can go through a percolation transition when either the concentration of droplets or temperature is varied. If the location of the percolation threshold is a slowly varying function of the temperature, identical exponents are expected whether or not the temperature or the droplet concentration is changed [5,6,11,16]. In the case of a variation of the number of droplets, at constant temperature (in the actual case, a ϕ variation), the increase of the droplets number leads to the formation of droplet clusters (dynamic percolation) or to the coalescence of droplets in continuous water channels (static percolation).

II. THEORETICAL MODEL

It is generally assumed that a water-in-oil microemulsion is made of two components, a dispersed water phase (1) and a continuous oil phase (2). The microemulsion complex permittivity ϵ^* [5,6,11] may be assumed to be a function of the complex permittivities of the dispersed phase, ϵ_1^*, and of the continuous phase, ϵ_2^*, where $\epsilon_i^*=\epsilon_{is}-j\sigma_i/(\omega\epsilon_o)$ for $i=1$ and 2. The two components are dielectric conductors with static permittivity ϵ_{1s} and ϵ_{2s} and conductivity σ_1 and σ_2; ϵ_o is the permittivity of vacuum; $\omega=2\pi f$; f is the frequency and $j^2=-1$.

In our case the oil Ohmic conductivity σ_2 is very close to zero, and the oil static dielectric constant is $\epsilon_2=1.8$. Furthermore, in the frequency range investigated, water and oil do not exhibit dielectric absorption, thus $|\epsilon_1^*|\gg|\epsilon_2^*|$.

The general relationship for the microemulsion complex permittivity ϵ^* is

$$\frac{\epsilon^*}{\epsilon_1^*}=|\phi-\phi_p|^{\mu}f\left(\frac{\epsilon_2^*/\epsilon_1^*}{|\phi-\phi_p|^{(\mu+s)}}\right), \tag{1}$$

where ϕ_p is the concentration percolation threshold, and μ and s (both greater than zero) are the percolation exponents [11]. Except in the neighborhood of ϕ_p, where the argument of the function f diverges, f satisfies the asymptotic forms reported in Ref. [11]. In our case, the argument of f is positive and lower than 1, thus a first-order expansion of f leads to the following asymptotic relationships for the microemulsion static dielectric constant (ϵ_s) and the conductivity (σ):

$$\epsilon_s=c_2\epsilon_{2s}(\phi_p-\phi)^{-s} \quad \text{below threshold,} \tag{2}$$

$$\sigma=c_2\sigma_2(\phi_p-\phi)^{-s} \quad \text{below threshold,} \tag{3}$$

$$\epsilon_s=c_1'\epsilon_{2s}(\phi-\phi_p)^{-s}+c_1\epsilon_{1s}(\phi-\phi_p)^{\mu} \quad \text{above threshold,} \tag{4}$$

$$\sigma=c_1'\sigma_2(\phi-\phi_p)^{-s}+c_1\sigma_1(\phi-\phi_p)^{\mu} \quad \text{above threshold,} \tag{5}$$

where c_1, c_1', and c_2 are constants. Below threshold [Eqs. (2) and (3)], ϵ_s and σ as functions of the difference $\phi_p-\phi$ follow a simple exponential law with an identical exponent, s; above threshold [Eqs. (4) and (5)], different trends can occur, depending on the value of constants c_1' and c_1 and of ϵ_{2s}, ϵ_{1s}, σ_1, and σ_2. Thus curve $\epsilon_s(\phi)$, at threshold, may either present a maximum or a maximum followed by a more or less pronounced minimum. The curve $\sigma(\phi)$ can present the same trend of the $\epsilon_s(\phi)$ curve. In practice, the weight of the term proportional to $(\phi-\phi_p)^{\mu}$ depends on the ratio $c_1'\epsilon_{2s}/(c_1\epsilon_{1s})$ in the case of Eq. (4), and on the ratio $c_1'\sigma_2/(c_1\sigma_1)$ in the case of Eq. (5), respectively. For our system the ratio $\epsilon_{2s}/\epsilon_{1s}$ is small, but finite ($\sim 1/40$), whereas σ_2/σ_1 is very close to zero as the perfluoropolyether oil is an excellent insulator. Thus, above threshold, in the $\sigma(\phi)$ relationship we expect that the second term dominates.

The conductivity as well as the static dielectric constant scaling laws as a function of $|\phi-\phi_p|$ are characterized by two critical exponents μ and s: $\mu=1.5$–2 for both static and dynamic percolation, while $s=0.6$–0.7 for static and $s\sim 1.2$ for dynamic percolation [5,6,8–19].

To describe the frequency dependence of the microemulsion complex permittivity at percolation, we recall that a theory on random resistor networks near their percolation threshold [22] was modified to describe quite well some microemulsions at percolation [9]. For the conductor-insulator mixture, the frequency dependence of the complex permittivity takes the form:

$$\epsilon^*(\omega)=E\omega^{u-1}\exp[j\pi(1-u)/2], \tag{6}$$

where E is real and u is a critical exponent. Equation 6 implies that both the real and imaginary parts of ϵ^*, $\epsilon'(\omega)$ and $\epsilon''(\omega)$ respectively, exhibit a ω^{u-1} frequency dependence, and that the loss angle Δ defined by $\tan\Delta(\omega)=\epsilon''(\omega)/\epsilon'(\omega)$ is independent of frequency and equal to $\pi(1-u)/2$, close to percolation threshold. Furthermore, the exponent u is related to μ and s by the equation $u=\mu/(\mu+s)$. Values of u between 0.56 and 0.63 are expected for dynamic percolation, and between 0.68 and 0.77 for static percolation. These values lead to loss angle tangent values of 0.69–0.58 and of 0.50–0.36 for dynamic and static percolation, respectively. We have to point out that the microemulsion differs from the conductor-insulator mixture. In fact, the sample conductivity at low ϕ is zero for the conductor-insulator mixture, and different from zero for the microemulsion sample because of the mechanism of charge carriers hopping between droplets, mechanism that cannot occur, for example, when metallic particles are dispersed in an insulating matrix. Moreover, in microemulsion, ϕ cannot increase up to 1.0 as in the conductor-insulator mixture. The polarization of aqueous droplets and of droplet clusters is similar to the polarization of the metallic particles, and of the particle clusters of the conductor-insulator mixture, respectively. Conversely, interdroplet exchange of matter and the aggregation processes of droplets are typical of microemulsions. Thus the above considerations related to conductor-

insulator mixtures apply, in microemulsions, in a frequency range which is characteristic of the microemulsion system investigated [9].

III. EXPERIMENT

The samples were obtained by a unique matrix with $\phi=0.6003$. The latter was prepared by mixing the water, the oil and the surfactant in proportions suitable to get a W/S=11 molar ratio. To solubilize the surfactant, the matrix was maintained at 80 °C for 3 h [2], and thereafter stabilized at room temperature. Each sample was prepared at room temperature in a different glass tube by addition of oil to a given amount of the matrix and then was studied after a stabilization at room temperature of at least one day. PFPE compounds were from Ausimont S.p.A., Milan (Italy). Water was taken from a Millipore Milli-Q system. The measured value of the water conductivity in the measuring cell was 42 μS/m at room temperature (measured with a resolution of 0.24 μS/m).

The apparatus for the dielectric investigation is composed of a low-frequency HP4192A impedance meter (frequency range 0.5 Hz to 13 MHz). The impedance meter is connected to a low frequency measuring cell which was described in Ref. [23]. The sample holder cell and the calibration procedure were described in detail in Ref. [23]. The temperature was controlled within ± 0.05 °C. Electrode polarization effects were detected in the low-frequency range, as described in Ref. [23]. The results reported in this paper are not affected by the electrode polarization except when explicitly mentioned. The low-frequency cell was built to stabilize the sample rapidly in the thermal range of interest 0–50 °C. The cell was filled with the sample at room temperature, then it was stabilized at the lowest temperature of the measurement and the temperature was increased by steps of a few degrees. A stabilization time of 5–10 min was found to be sufficient to achieve the equilibrium. At any frequency tested, the measured parameters were the impedance magnitude and the phase angle of the dielectric cell filled with the sample.

IV. RESULTS

A. Analysis as a function of concentration

The behavior of the static dielectric constant vs ϕ in the temperature range 5–38 °C is reported in Fig. 1. Different trends, depending on the temperature interval analyzed, are shown. Below 16 °C, the static dielectric constant increases as a function of increasing ϕ. Above 16 °C and below 20 °C, a well-defined peak occurs at $\phi\sim 0.45$. Above 20 °C and below 26 °C two badly resolved maxima are shown at $\phi_1\sim 0.45$ and $\phi_2\sim 0.35$, respectively, whereas at higher temperatures only one maximum, less and less pronounced, is shown at $\phi\sim 0.36$. The explanation of this behavior can be found in the change of the ratio $c_1'\epsilon_{2s}/(c_1\epsilon_{1s})$ as a function of temperature (see Sec. II).

In Fig. 2 the conductivity as a function of ϕ is reported in the range 10–40 °C. For all temperatures, the conductivity increases as a function of ϕ. The sigmoidal shape, typical of the percolative $\log[\sigma(\phi)]$ dependence, can be recognized only at intermediate temperatures. The data set of Figs. 1 and 2, that describes the behavior of $\epsilon_s(\phi)$ and $\sigma(\phi)$ at different temperatures, corresponds to the data set analyzed in Ref. [1] as a function of temperature at different ϕ.

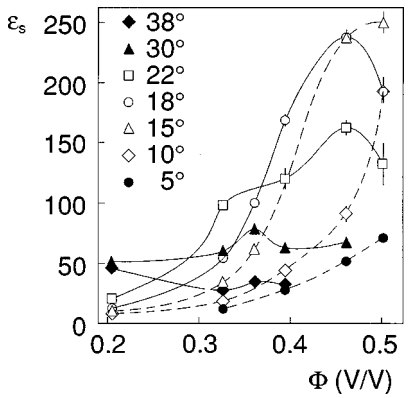

FIG. 1. Experimental $\epsilon_s(\phi)$ values at different temperatures. Dashed lines at 5, 10, and 15 °C. Continuous lines at 18, 22, 30, and 38 °C. The lines are guides for the eyes.

The data of Fig. 2 do not allow one to determine the threshold value ϕ_p. To detect ϕ_p a series of measurements was carried out at 20 and 25 °C (see Fig. 3). In Fig. 4 the scaling behavior of the $\log_{10}(\sigma)$ vs $\log_{10}|\phi-\phi_p|$ is plotted for the data above and below the threshold value at which the curvature of the function $\log_{10}[\sigma(\phi)]$ inverts. The analysis has given the following results: at $T=20$ °C, $\phi_p=0.401\pm 0.002$, and the critical exponents are $\mu=1.74\pm 0.05$ and $s=1.48\pm 0.03$. At $T=25$ °C, $\phi_p=0.346\pm 0.002$ and $\mu=1.62\pm 0.05$. The s exponent cannot be estimated in the latter case.

For $\epsilon_s(\phi)$ curves, the ϕ value at which the maximum occurs (see Fig. 1) in some cases is not clearly evident, while in other cases it is well defined, but the resolution is poor because the points are far apart; in other cases the analysis above threshold is not possible because the curves exhibit a superposition of two maxima. Nevertheless, we performed a data analysis below threshold at $T=20$ °C, assuming as threshold the value obtained from the conductivity study. The plot of $\log_{10}(\epsilon_s)$ as a function of $\log_{10}(\phi_p-\phi)$ is re-

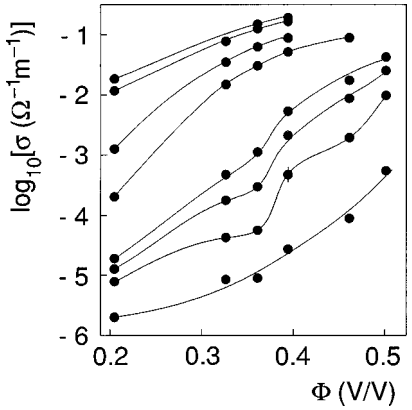

FIG. 2. Experimental $\sigma(\phi)$ values at different temperatures. From bottom to top in the picture: $T=10$, 15, 18, 20, 28, 32, 38, and 40 °C. The curves show the crossing of ϕ_p threshold (sigmoidal shape curve) at 15, 18, and 20 °C, the trend above ϕ_p at higher temperatures (upper part of the sigmoidal shape curve) and the trend below ϕ_p at the lowest temperature. The lines are guides for the eyes.

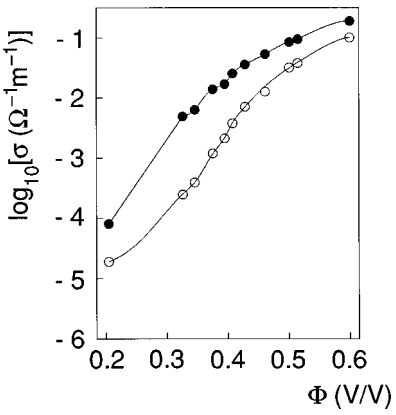

FIG. 3. Experimental $\sigma(\phi)$ values at $T=20\,^{\circ}\mathrm{C}$ (open points) and $T=25\,^{\circ}\mathrm{C}$ (full points). The lines are guides for the eyes.

ported in Fig. 5. The scaling behavior is shown, and an exponent $s=1.18\pm0.04$ has been calculated. A further investigation was performed on data below threshold at $T=16$ and 18 °C, by assuming as threshold ϕ_p different values in the interval from 0.41 to 0.46 (see Fig. 1). The latter study leads to the conclusion that s values lower than 1.1 can be excluded.

In summary, in the thermal range 5–15 °C, the $\epsilon_s(\phi)$ and $\sigma(\phi)$ curves show an increasing trend but the threshold is not reached, thus no estimation of the critical exponents can be done. At 16 and 18 °C, the threshold can be approximatively estimated from the $\epsilon_s(\phi)$ dependence, and the s exponent, found below threshold, is that of dynamic percolation. At 20 °C the threshold can be found by the $\sigma(\phi)$ dependence: $\phi_p=0.40$. From both $\epsilon_s(\phi)$ and $\sigma(\phi)$ the s exponent below threshold is that of dynamic percolation. At 25 °C, from the $\sigma(\phi)$ curve, the percolation threshold is $\phi_p=0.35$, but only the exponent above threshold can be calculated. We point out that the ϕ_p threshold decreases from 0.40 to 0.35 as the temperature increases from 20 to 25 °C.

B. Analysis as a function of frequency

(i) Constant temperature and different concentrations. The behavior of both the real and imaginary parts of the complex permittivity vs frequency is reported in Figs. 6(a) and 6(b), at 20 °C, for samples with ϕ in the range from 0.2 up to 0.6. A

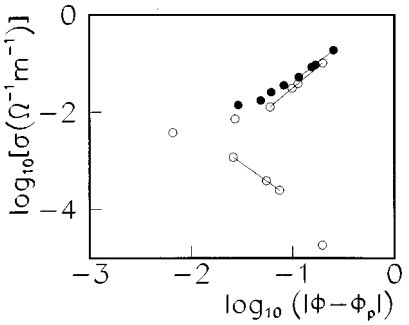

FIG. 4. Experimental values of Fig. 3 arranged to show the linear trend of the $\log_{10}(\sigma)$ vs $\log_{10}|\phi-\phi_p|$ below (bottom curve) and above (upper curves) the percolation threshold. The straight lines represent the fitting results. The symbol meanings are as in Fig. 3.

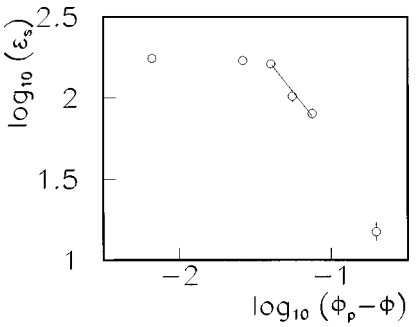

FIG. 5. Experimental values of Fig. 1 at 20 °C showing the linear trend $\log_{10}(\epsilon_s')$ vs $\log_{10}(\phi_p-\phi)$, below the percolation threshold.

similar behavior was observed at $T=25\,^{\circ}\mathrm{C}$. The curves of Fig. 6(a) show that $\epsilon'(f)$ decreases as f increases; the slope of the curves depends on ϕ and becomes smaller as ϕ decreases. The corresponding $\epsilon''(f)$ curves, Fig. 6(b), show a broad asymmetrical maximum which shifts toward lower frequencies for intermediate values of ϕ. In agreement with Eq. (6), a linear trend of $\log_{10}(\epsilon')$ vs $\log_{10}(f)$ was observed in the frequency interval from 10^6 to 10^7 Hz, for some of the samples studied at $T=20$ and 25 °C [see Figs. 7(a) and 7(b)]. Values of the exponent u, which are typical of dynamic percolation, were obtained (see Table I) at 20 °C in the ϕ range 0.515–0.408, and at 25 °C in the ϕ range 0.408–0.327. A similar analysis was reported in Ref. [24] for the sample with $\phi=0.462$ at 20 °C. The above findings are in good agreement with the theoretical predictions that, on

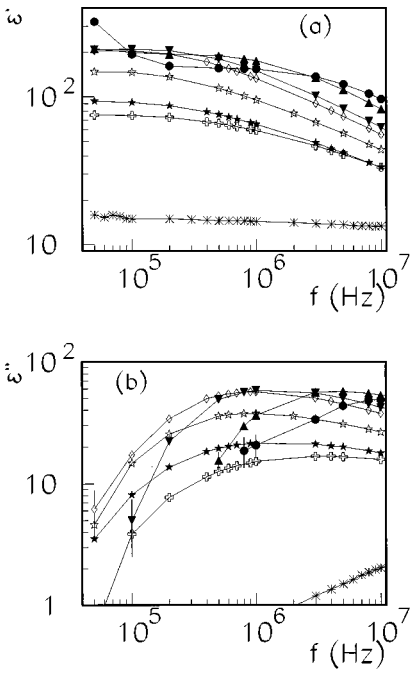

FIG. 6. $\epsilon'(f)$ and $\epsilon''(f)$ experimental values [(a) and (b), respectively], at $T=20\,^{\circ}\mathrm{C}$, for the samples with ϕ: 0.600 (full points), 0.515 (full triangles), 0.429 (full reversed triangles), 0.408 (open diamond), 0.361 (open stars), 0.346 (full stars), 0.327 (open crosses), and 0.205 (asterisks). The increase of ϵ' below 10^5 Hz at $\phi=0.600$ is due to electrode polarization. The lines are guides for the eyes.

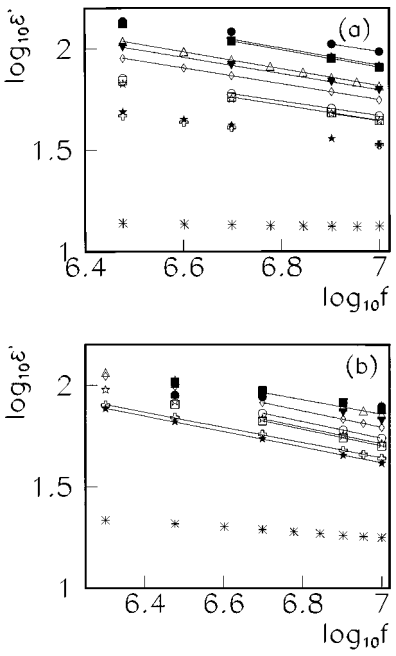

FIG. 7. The linear portion of $\epsilon'(f)$ in log-log scale at $T=20\,^{\circ}\mathrm{C}$ (a) and $T=25\,^{\circ}\mathrm{C}$ (b) for the samples with ϕ: 0.600 (full points), 0.515 (full triangles), 0.501 (full squares), 0.462 (open triangles), 0.429 (full reversed triangles), 0.408 (open diamond), 0.395 (open squares), 0.375 (open points), 0.361 (open stars) 0.346 (full stars), 0.327 (open crosses), and 0.205 (asterisks). The straight lines are the results of the fit.

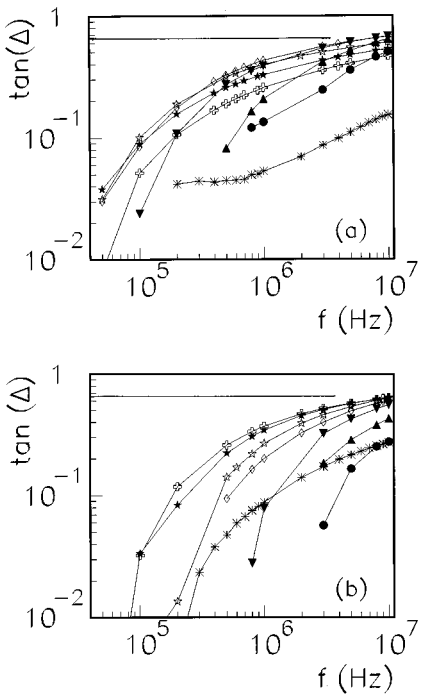

FIG. 8. Loss angle tangent vs frequency for the samples of Fig. 6, at $T=20\,^{\circ}\mathrm{C}$ (a) and $T=25\,^{\circ}\mathrm{C}$ (b), respectively. The line with constant $\tan\Delta=0.65$ is drawn. For clarity of the picture, the points affected by electrode polarization at $\phi=0.600$ and 0.515 are not reported. The symbol meanings are as in Fig. 6.

approximating the threshold value, in our case 0.40 at 20 °C and 0.35 at 25 °C, a linear trend must be observed in the dependence of $\log_{10}(\epsilon')$ vs $\log_{10}(f)$ (see Sec. II). The u values found are typical of dynamic percolation.

As a further confirmation of the above results, the behavior of $\tan(\Delta)$ vs frequency was also analyzed for the samples of Table I; the plot on a double-logarithmic scale is reported in Figs. 8(a) and 8(b) at 20 and 25 °C, respectively, for the samples of Fig. 6. In the frequency range where the double-logarithmic $\epsilon'(f)$ dependence is linear, we expect $\tan(\Delta)$ vs f to flatten at some frequency-independent value. As shown in Figs. 8(a) and 8(b), there is a frequency interval in which $\tan\Delta$ approximates the horizontal asymptote at 0.65. This value is representative of the dynamic percolation. It is achieved for the samples with $\phi\sim0.40$ at 20 °C and with $\phi\sim0.35$ at 25 °C. In summary, from the analysis of the real and imaginary parts of the microemulsion complex permittivity as a function of frequency, at 20 and 25 °C, for samples of the whole monophasic region, a percolation phenomenon of dynamic type is demonstrated to occur.

TABLE I. u exponents of the linear frequency dependence of $\log_{10}(\epsilon')$ vs $\log_{10}(f)$ for the samples of Fig. 6. For the two samples with $\phi=0.600$ and 0.205, no linear dependence was found in the frequency range studied. The errors reported in the table (and in the whole paper) are standard deviations. χ^2 values close to 1 were found in data analysis.

ϕ	T(°C)	u	T(°C)	u
0.600	20		25	
0.515	20	0.57±0.01	25	
0.501	20	0.57±0.01	25	
0.462	20	0.580±0.005	25	
0.429	20	0.590±0.007	25	
0.408	20	0.605±0.006	25	0.60±0.01
0.395	20		25	0.59±0.01
0.375	20		25	0.59±0.01
0.361	20		25	0.59±0.01
0.346	20		25	0.62±0.01
0.327	20		25	0.63±0.01
0.205	20		25	

(ii) Constant concentration and different temperatures. The study of the frequency dependence of the complex permittivity was also performed, at different temperatures, for each sample in the ϕ interval from 0.205 to 0.501. A typical result of the above analysis is reported in Figs. 9(a) and 9(b), for the sample with $\phi=0.462$. The real and the imaginary parts of the complex dielectric constant [Fig. 9(a)] and the loss angle tangent [Fig. 9(b)] vs frequency are reported in the temperature interval from -0.7 to 16.9 °C. A thermal threshold of 16.5 °C was found from the analysis of ϵ_s vs temperature, reported in Ref. [1]. Thus the curves of Figs. 9(a) and 9(b) cover the region below and up to the thermal threshold. In the frequency range from 10^6 to 10^7 Hz, straight lines were found in the double-logarithmic $\epsilon'(f)$ dependence. The u values calculated at three different temperatures close to the thermal threshold are reported in Table II. A similar study is reported in Ref. [24] for the sample with $\phi=0.327$ at 24 °C. In the same frequency interval, the double-logarithmic $\tan(\Delta)$ vs f curves of Fig. 9(b) show a flattening to the value of 0.67, as the temperature increases up to 16.9 °C. The curves at higher temperature, not reported

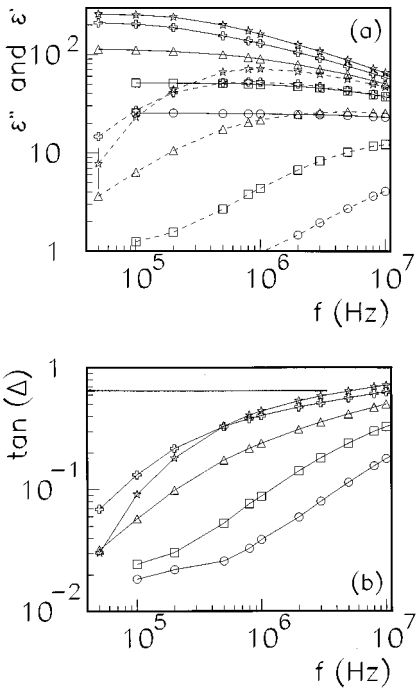

FIG. 9. Real (continuous lines) and imaginary (dashed lines) part of the complex dielectric constant (a) and loss angle tangent (b) vs frequency, for the sample with $\phi = 0.462$ at the temperatures: -0.7 °C (points), 6.1 °C (squares), 11.1 °C (triangles), 14.0 °C (crosses), and 16.9 °C (stars). The line is $\tan\Delta = 0.65$.

for clarity of the picture, stay below this value. In Table II the results are reported for all the samples studied. The critical exponent u and the $\tan(\Delta)$ values at the percolation threshold are typical of dynamic percolation. The only parameters of Table II, which are intermediate between the value of static and dynamic percolation, are those at $\phi = 0.205$. To clarify this point, in Fig. 10 we report the double-logarithmic $\tan\Delta(f)$ curves at $\phi = 0.205$. The higher curve is observed at 34 °C (the range of the figure is 30–40 °C), and the derivative of $\tan\Delta(f)$ at the higher frequencies is positive, so that the curve will flatten to a value higher than 0.56 (reported in Table II) at frequencies higher than those explored. A dynamic percolation exponent is expected to be found also for this sample at frequencies higher than 10^7 Hz.

TABLE II. u exponents of the linear frequency dependence of $\log_{10}(\epsilon')$ vs $\log_{10}(f)$ and loss angle tangent at percolation threshold, for samples studied at different temperatures. The errors are standard deviations. χ^2 values close to 1 were found in data analysis. The thermal thresholds T_d are taken from Ref. [1].

ϕ	T(°C)	u	tanΔ	T_d(°C)
0.501	12	0.60±0.01	0.62±0.01	13.0
	14	0.57±0.01	0.68±0.01	
0.462	15	0.62±0.01		16.5
	16	0.60±0.01		
	16.9	0.61±0..01	0.67±0.01	
0.395	17	0.64±0.01		18.9
	18	0.63±0.01	0.65±0.01	
	20	0.61±0.01	0.65±0.01	
0.361	23	0.64±0.01	0.65±0.01	21.6
0.327	24	0.62±0.01	0.65±0.01	22.8
	26	0.62±0.01		
0.205	34	0.65±0.01	0.56±0.01	32.4

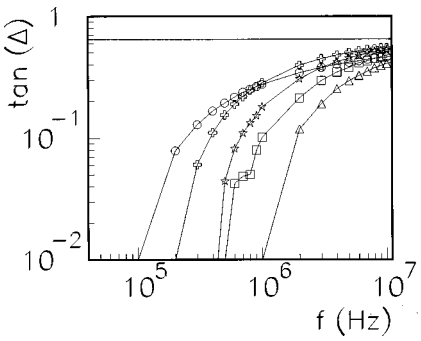

FIG. 10. Loss angle tangent vs frequency for the sample with $\phi = 0.205$, at temperatures 30 °C (points), 34 °C (crosses), 36 °C (stars), 38 °C (squares), and 40 °C (triangles). The line is $\tan\Delta = 0.65$.

V. DISCUSSION

From the results of this paper, the percolation phenomenon of perfluoropolyether microemulsions with W/S=11 was found to be of dynamic type. At 20 °C the concentration threshold is reached with a volume fraction of the dispersed phase $\phi_p = 0.40$, at 25 °C with $\phi_p = 0.35$. Both values are lower than the hard-sphere close-packing limit, which is 0.65, and this indicates that the interfacial surfactant layers of the droplets interpenetrate significantly. The exponents $\mu \simeq 2$ and $s \simeq 1.2$, typical of dynamic percolation, were found by studying the dependence of the static dielectric constant and conductivity as a function of ϕ. The study as a function of frequency leads to u exponents and $\tan\Delta$ values typical of a dynamic percolation, both for the samples studied at the constant temperatures of 20 and 25 °C with ϕ in the range from 0.205 to 0.600 and, as a function of temperature, in the corresponding ϕ interval. The analysis of the temperature dependence of both ϵ_s and σ in the range from 0 to 40 °C, reported in Ref. [1] for samples with ϕ in the interval from 0.205 to 0.501, showed a dynamic percolation phenomenon for all the samples below the respective thermal thresholds and, above thresholds, except at $\phi = 0.205$, 0.327, and 0.501. To facilitate the comparison between the results of this work and those of Ref. [1], the percolative thermal thresholds calculated in Ref. [1] are reported in the right column of Table II. For all samples, the threshold we found as the temperature at which the maximum of the $\epsilon_s(T)$ curve occurs, belongs to the thermal range in which $\epsilon'(f)$, in log-log scale, show the linear dependence vs frequency, and $\tan(\Delta)$ achieves a constant value. Furthermore, close to the dielectric threshold T_d, u and $\tan(\Delta)$ have the values of dynamic percolation. In particular, above threshold at $\phi = 0.501$, 0.327, and 0.205, dynamic percolation values for u and $\tan(\Delta)$ were found. The latter finding excludes that static percolation could occur above threshold for the samples with $\phi = 0.501$, 0.327, and 0.205. Thus a reconsideration of the data of Ref. [1], as a function of temperature, has shown that in Ref. [1] we found static exponents because we used too large a temperature

interval; this was a consequence of having overestimated error bars. In fact, a recalculation of the exponents in the $\epsilon_s(T)$ dependence above the thermal threshold at $\phi=0.501$, 0.327, and 0.205, gives $s\sim1.2$, a value again typical of dynamic percolation.

To have a further confirmation of the above findings, a study of small angle neutron scattering (SANS) is in progress. Preliminary results at W/S=11 with temperatures of 25 and 35 °C [25], have shown that, at $\phi=0.205$ the microemulsion sample is composed of droplets having a core radius of 23 Å. At $\phi=0.205$, the thermal threshold is in between 20 and 35 °C. Therefore, at $\phi=0.205$ we can further exclude that static percolation occurs above threshold. The value of 23 Å, obtained by SANS, is in good agreement with the hydrodynamic radius of 31 Å found by quasielastic light scattering (QELS). The difference is due to the fact that by SANS, because of the contrast [25], we measure the aqueous core radius, whereas by QELS we measure the hydrodynamic radius of the whole droplet. By SANS, the area per surfactant molecule at interface was also calculated [25]. The value, 50 $Å^2$, remains constant from $\phi=0.0205$ up to $\phi\sim0.25$ at both 20 and 35 °C, indicating that the surfactant packing is the same throughout a wide ϕ range from 2% to 25% of the dispersed phase, below (20 °C) and above (35 °C) the thermal percolation threshold of these samples. Further SANS data analysis is in progress to obtain information on the whole structural evolution along the line W/S=11.

Another interesting feature to be noticed on the percolation phenomenon described in this paper is the variation of ϕ_p from 0.40 to 0.35 as the temperature is increased from 20° to 25°C and the increase of the thermal threshold as ϕ decreases. To gain a better insight into the threshold variation, we report that, at W/S=12 a percolative trend, similar to that observed at W/S=11, was also found. The percolation threshold at W/S=12 and $T=20$ °C is $\phi_p=0.25$. The critical exponents of the $\epsilon_s(\phi)$ and $\sigma(\phi)$ dependence are $\mu\sim2$ and $s\sim1.1$ [26]; the values are typical of dynamic percolation. We point out that ϕ_p is significantly reduced for a small W/S increase. The percolation threshold ϕ_p is very sensitive to temperature and to W/S changes, as reported for other microemulsions [11,12,14,17]. Furthermore, at W/S=0.35 and 0.39 w/w (molar ratios 14 and 16, respectively), the static dielectric constant increases as a function of ϕ up to very high values (in Ref. [27] these values can be deduced by the frequency relaxation spectra) when ϕ approximates 0.59, which is close to the boundary of the monophasic region. Calculation of percolation thresholds and critical exponents cannot be performed. However, we can deduce that the percolation threshold at W/S=14 and 16 is close to the phase separation boundary, which is also very near to the hard-sphere close-packing limit. Work is in progress to analyze the dielectric results outside the W/S=11 line.

VI. CONCLUSION

Percolation occurs in fluorinated water-in-oil microemulsions. On the basis of a preliminary investigation, the study has been performed at water to surfactant ratio W/S=11, which is the most suitable value to detect the percolation threshold and to calculate the critical exponents below and above threshold. In the whole concentration range and temperature interval where monophasic microemulsions exist, the exponents found are characteristic of a dynamic percolation phenomenon. The interactions between droplets play the role of maintaining droplets, in the system, up to the higher volume fraction of dispersed phase, 60%. The droplets cores remain well defined either at different concentrations or at different temperatures. However the exchanges of ions species between droplets are favored by the ability of the interfacial layers to interpenetrate significantly, which indicates that the interface is composed of a highly flexible film.

ACKNOWLEDGMENTS

The authors acknowledge useful discussions on percolation theory with R. Livi, and thank Dr. P. Gavezzotti for the preparation of surfactants. This work was supported by Ausimont S.p.A. and by MURST and INFM funds. M.G.G. thanks Ausimont for support during this research work.

[1] M. G. Giri, M. Carlà, C. M. C. Gambi, D. Senatra, A. Chittofrati, and A. Sanguineti, Phys. Rev. E **50**, 1313 (1994).
[2] A. Chittofrati, D. Lenti, A. Sanguineti, M. Visca, C. M. C. Gambi, D. Senatra, and Z. Zhou, Prog. Colloid Polym. Sci. **79**, 218 (1989).
[3] A. Sanguineti, A. Chittofrati, D. Lenti, and M. Visca, J. Colloid Interface Sci. **155**, 402 (1993).
[4] In Ref. [1], at the end of page 1313, ''low oil content'' should be changed to ''low water content.''
[5] S. A. Safran, I. Webman, and G. S. Grest, Phys. Rev. A **32**, 506 (1985).
[6] G.S. Grest, I. Webman, S. A. Safran, and L. R. Bug, Phys. Rev. A **33**, 2842 (1986).
[7] M. Lagues, R. Ober, and C. Taupin, J. Phys. (France) Lett. **39**, 487 (1978).
[8] M. A. Van Dijk, Phys. Rev. Lett. **55**, 1003 (1985).
[9] M. A. Van Dijk, G. Casteleijn, J. G. H. Joosten, and Y. K. Levine, J. Chem. Phys. **85**, 626 (1986).
[10] J. Peyrelasse, M. Moha-Ouchane, and C. Boned, Phys. Rev. A **38**, 904 (1988).
[11] J. Peyrelasse and C. Boned, Phys. Rev. A **41**, 938 (1990).
[12] C. Cametti, P. Codastefano, A. Di Biasio, and P. Tartaglia, Phys. Rev. A **40**, 1962 (1989).
[13] C. Cametti, P. Codastefano, P. Tartaglia, J. Rouch, and S.-H. Chen, Phys. Rev. Lett. **64**, 1461 (1990).
[14] C. Cametti, P. Codastefano, P. Tartaglia, S.-H. Chen, and J. Rouch, Phys. Rev. A **45**, R5358 (1992).
[15] M. A. Knackstedt, B. W. Ninham, Phys. Rev. E **50**, 2839 (1994).
[16] C. Mathew, Z. Saidi, J. Peyrelasse, and C. Boned, Phys. Rev. A **43**, 873 (1991).
[17] C. Boned, J. Peyrelasse, and Z. Saidi, Phys. Rev. E **47**, 468 (1993).

[18] C. Boned, Z. Saidi, P. Xans, and J. Peyrelasse, Phys. Rev. E **49**, 5295 (1994).
[19] H. F. Eicke, W. Meier, and H. Hammerich, Langmuir **10**, 2223 (1994).
[20] H. F. Eicke, M. Borkovec, and D. DasGupta, J. Phys. Chem. **93**, 314 (1989).
[21] Y. Feldman, N. Kozlovich, I. Nir, and N. Garti, Phys. Rev. E **51**, 478 (1995).
[22] J. M. Luck, J. Phys. A **18**, 2061 (1985).
[23] M. G. Giri, M. Carlà, C. M. C. Gambi, D. Senatra, A. Chittofrati, and A. Sanguineti, Meas. Sci. Technol. **5**, 627 (1993).
[24] M. G. Giri, M. Carlà, C. M. C. Gambi, D. Senatra, A. Chittofrati, and A. Sanguineti, Prog. Colloid Polym. Sci. **100**, 182 (1996).
[25] P. Baglioni, C. M. C. Gambi, R. Giordano, and D. Senatra, J. Mol. Struct. **383**, 165 (1996).
[26] Unpublished results.
[27] M. G. Giri, M. Carlà, C. M. C. Gambi, D. Senatra, A. Chittofrati, and A. Sanguineti, IEEE Trans. Dielectr. Electr. Insul. **1**, 716 (1994).